lubricants

MDPI

Article

Experimental Research on the Effect of Thermophysical Characteristics of Cutting Fluid on Cutting Performance During Turning Ti-6Al-4V Alloy

Xiaorong Zhou [1,2], Lin He [2,*], Sen Yuan [3], Jing Deng [2], Zebin Su [2], Jingdou Yang [2] and Feilong Du [2]

[1] School of Mechanical Engineering, Guiyang University, Guiyang 550005, China
[2] School of Mechanical Engineering, Guizhou University, Guiyang 550025, China
[3] School of Mechanical Engineering, Guizhou Institute of Technology, Guiyang 550003, China
* Correspondence: helin6568@163.com

Abstract: Cutting fluid has been widely used to enhance the heat dissipation of cutting systems. However, whether cutting fluid can fully play its role is closely correlated with its thermophysical characteristics, such as viscosity, surface tension, etc. In this work, to study the effect of the thermophysical characteristics of cutting fluid on cutting performance, three green vegetable oils (semi-synthetic fluid (L1), rapeseed oil (L2), canola oil (L3)) were selected as cutting fluids of the MQL system, and differences in cutting performance were compared and analyzed under varied lubrication environments. Firstly, the thermophysical characteristics of the vegetable oils were determined by experimental methods. Afterwards, parameters, including tool wear, cutting force, and temperature, as well as the quality of machined workpieces, were selected to evaluate cutting performance, and essential reasons for the difference in cutting performance under varied lubrication environments were clarified. The results demonstrated that the cutting force, cutting temperature, and tool wear produced in the three MQL environments were lower than those in the dry cutting environment, while only the L1 and L2 MQL environments exhibited higher machined surface quality than the dry cutting environment. Moreover, obvious differences in cutting performance under the three MQL environments were also observed due to the different thermophysical characteristics of the three vegetable oils. The best cutting performance was achieved when L2 was used as the MQL cutting fluid. The efforts of this study will give an important reference for the choosing of green cutting fluid in the cutting process of difficult-to-cut materials and be of great significance for accelerating the development of green processing.

Keywords: MQL; vegetable oil; thermophysical characteristics; Ti-6Al-4V alloy; cutting performance

check for updates

Received: 30 December 2024
Revised: 26 January 2025
Accepted: 8 February 2025
Published: 17 February 2025

Citation: Zhou, X.; He, L.; Yuan, S.; Deng, J.; Su, Z.; Yang, J.; Du, F. Experimental Research on the Effect of Thermophysical Characteristics of Cutting Fluid on Cutting Performance During Turning Ti-6Al-4V Alloy. *Lubricants* **2025**, *13*, 90. https://doi.org/10.3390/lubricants13020090

Copyright: © 2025 by the authors. Licensee MDPI, Basel, Switzerland. This article is an open access article distributed under the terms and conditions of the Creative Commons Attribution (CC BY) license (https://creativecommons.org/licenses/by/4.0/).

1. Introduction

Green growth and low-carbon sustainable development are the common goals of many countries across the world. With the continuous exploitation and utilization of resources, resource shortages and environmental pollution have become increasingly prominent, and they are currently the two major obstacles on the road towards sustainable development. To alleviate resource shortages and environmental issues, the dual carbon goals (carbon peak and carbon neutral) have been highly valued by the world, and the concept of "green manufacturing" has been introduced into the industrial field worldwide. To contribute

to the realization of the dual carbon goals and to follow the concept of "green manufacturing", the cutting industry, as a typical area of the manufacturing field, has proposed the development goal of "clean cutting". Currently, a big problem in the cutting process is the increase in cutting temperature and the consequent reduction in cutting performance. This problem is more prominent during processing the difficult-to-cut material. The traditional method to address the above issue is to use a large amount of cutting fluid, and the reduction in cutting temperature is achieved through the cooling and lubrication of cutting fluid [1]. However, the extensive use of cutting fluid not only causes resource waste but also poses a serious threat to the health of the operator and the sustainable development of the environment [2,3]. Therefore, how to balance the cutting performance and clean cutting concept for difficult-to-cut materials becomes a research focus of the cutting industry.

In recent years, MQL technology has received increasing attention from the perspective of both scientific research and industrial application [4,5]. Extensive efforts have been made to determine the effects of MQL on cutting performances. For example, Tian et al. [6] conducted a study on processing the Inconel 718 superalloy with carbide tools coated with AlCrN under dry cutting and MQL environments and found that compared to dry cutting, the introduction of MQL could not only effectively prolong the lifetime of the tool but also inhibit burr generation and enhance the workpiece's surface quality. Aslan et al. [7] compared and analyzed the performance of the coated carbide tool during the milling of structural steel Strenx900 under dry and MQL environments. The results showed that the MQL environment could effectively alleviate tool flank wear and reduce cutting energy and workpiece surface roughness. In addition, Sirin et al. [8] reported that during milling the X-750 nickel alloy with ceramic SiAlON tools, higher machined surface quality and smaller cutting force were observed under the MQL environment than in the dry cutting condition. However, tool wear that occurred in the MQL environment was more serious compared to that in the dry cutting environment. This was attributed to the generation of a built-up edge on the tool surface in the process of dry cutting, which reduced the friction and wear of the tool, thus enhancing the wear resistance of the tool in the dry cutting environment.

Under the guidance of the concept of green machining and clean cutting, in addition to the application of promising MQL technology instead of the traditional pouring cooling lubrication method, relevant research has also focused on the replacement of traditional mineral oil with green and environmentally friendly biodegradable bio-oils [9–12]. Singh et al. [13] carried out turning experiments of the alloy Ti-6Al-4V with cemented carbide tools in both the dry condition and MQL environment using canola oil as the cutting fluid. The experimental results indicated that in comparison with the dry cutting environment, tool wear could be alleviated to a certain extent by using canola oil. Yuan et al. [14] synthesized a new green vegetable oil with castor oil and ethanol in a certain proportion and conducted the experiment of the cemented carbide tool, turning the Ti-6Al-4V bar in dry cutting, pouring cutting, and MQL conditions. The results demonstrated that in comparison with dry cutting, using the synthetic mixed vegetable oil as cutting fluid led to a decrease in tool flank wear and the machined surface roughness by 38% and 36%, respectively. The corresponding reduction values in comparison with the pouring cutting were 53% and 15%, respectively. Gaurav et al. [15] pointed out that the vegetable jojoba oil could be used as a cutting fluid for turning the Ti-6Al-4V alloy under the MQL environment, where the tool wear, cutting force, and roughness of the workpiece surface were effectively reduced compared to that in the dry cutting environment.

In addition to the comparison of cutting performance in the dry cutting and MQL conditions, the influences of the MQL parameters on the flow characteristics of cutting fluid droplets have also been studied in some works. Du et al. [16] used the computational fluid dynamics (CFDs) method to study the influences of varied nozzle pose parameters on

the characteristics of cutting fluid droplets and verified the lubrication and cooling effects of cutting fluid under different nozzle pose parameters through milling experiments of 316L stainless steel. It was found that the problem of insufficient lubrication or excessive lubrication could be avoided by placing the nozzle at the optimal injection distance. Moreover, the wear degree of the tool and the roughness of the machined workpiece surface were reduced to a certain extent by spraying the cutting fluid in the direction of 45°. To analyze the effects of injection pressure, nozzle diameter, as well as flow rate on the spray characteristics of the cutting fluid, Subramani and Muthu et al. [17] established a discrete phase model (DPM) of rapeseed oil under different MQL parameters using ANSYS Fluent 19 R1 software. They observed that the nozzle diameter and the flow rate had little effect on the particle diameter, but a larger nozzle diameter and higher flow rate could increase the particle velocity. In addition, a smaller particle diameter and larger particle velocity could be obtained by increasing the injection pressure. El-Bouri et al. [18] studied the influences of inlet pressure (1, 3, and 5 bar) and flow rate (50–200 mL/h) on the maximum temperature of the tool using the CFDs model during turning difficult-to-machine materials in the MQL environment. It was found that the MQL mass flow rate had little effect on the average temperature value of the tool rake face, while the increase in the inlet pressure could reduce the tool average temperature.

In the MQL environment, the cooling and lubrication effects of cutting fluids are not only related to MQL injection parameters but also correlated with the types of cutting fluids. Each cutting fluid has its unique characteristic, and different cutting fluids can result in varied interactions between cutting fluids and tool surface, which further affects cutting performance. Saleem and Mehmood [19] analyzed the differences in cutting performance under dry cutting and MQL environments with sprayed sunflower oil and castor oil in the process of turning Inconel superalloy 718 using Tialn PVD-coated tools. The results suggested that the roughness of the workpiece surface and the wear of the tool in the two MQL environments were smaller than those in the dry cutting process, and sunflower oil showed better lubrication and cooling performances than castor oil. In the process of grinding nickel-based superalloy GH4169 under MQL environments, Guo et al. [20] compared the grinding forces of pure castor oil and castor oil mixed with oils from sunflower, rapeseed, palm, soybean, maize, and peanut. It was found that the mixed oil generated a smaller grinding force compared to pure castor oil, and the mixed oil of castor and soybean exhibited the highest capability for grinding force reduction. Pal et al. [21] investigated the effects of distilled water and oils from sunflower, castor, coconut, palm, canola, and soybean on tool cutting performance during drilling stainless steel AISI321 in the MQL condition. In this experiment, the best lubrication performance was observed with the sunflower oil, which led to a lower friction coefficient, force, torque, and workpiece surface roughness compared to those in the pouring environment.

The above studies suggest that the lubrication and cooling effects of cutting fluids can be adjusted by changing the types and characteristics of the fluids in the MQL condition, thus affecting the performance of the cutting tool. Differently, Yin et al. [22] investigated the effect of the physical property performed by vegetable oil on the friction coefficient and surface roughness in the milling process of AISI 1045 under the MQL environment. It was found that a stronger lubrication effect was achieved using vegetable oil with a higher viscosity and smaller contact angle. Jamil et al. [23] explored the relationship between thermophysical properties (density, thermal conductivity, viscosity, specific heat) and temperature. They observed that an increase in temperature led to a decrease in density, viscosity, and thermal conductivity and an increase in specific heat and found that a higher viscosity was conducive to lubrication during the MQL milling process of Ti-6Al-4V. Nwoguh et al. [24] pointed out that a higher viscosity could give rise to a better

cutting performance during the machining process of Inconel 718 under MQL environments. However, previous studies on the thermophysical properties of cutting fluids focused on either contact angle or viscosity; comprehensive research on the thermophysical characteristics of cutting fluid is lacking during the turning process of Ti-6Al-4V under the MQL environment.

In this study, the effects of the thermophysical characteristics of cutting fluid on cutting performance were studied in the process of turning Ti-6Al-4V workpiece with the cemented carbide tool under different lubrication environments. Firstly, the initial boiling temperature, surface tension, and viscosity of several cutting fluids, as well as the contact angle of cutting fluid on the cutting tool surface, were determined by experimental methods. Afterwards, turning experiments were implemented under varied lubrication conditions, and the process parameters, including cutting force and temperature, were collected in real time. Finally, a white light interferometer was adopted to detect the three-dimensional (3D) topography of the machined workpiece surface, and the wear characteristics of the tools were analyzed with a scanning electron microscope (SEM) as well as an energy dispersive X-ray spectrometer (EDS). In addition, the mechanisms of tool wear were investigated based on the experimental results. The findings from this work contribute to the selection and development of high-performance green cutting fluids for processing difficult-to-cut material, which is of great significance for accelerating the conversion from traditional machining to green cutting.

2. Experimental Procedure and Methodology

2.1. Cutting Experiments and Corresponding Tests

To evaluate the effects of cutting fluid on the performances of the cutting tool, experiments of turning Ti-6Al-4V alloy were conducted on the C6136HK CNC lathe with a cemented carbide tool (TCMW 16 T304 H13A) under different cutting environments (dry and three MQL environments with different cutting fluids). The cutting force, cutting temperature, tool wear, and quality of the machined surface were used as the evaluation index to assess the performance of the cutting tool. Ti-6Al-4V alloy used here was obtained from enterprise and annealed, of which the relative properties are given in Table 1. The platform of the cutting experiments is shown in Figure 1. A STGCR2020K16 tool holder was used in the experiments. The rake angle, the cutting edge angle, and the clearance angle were 0°, 90°, and 7°, respectively. The cutting force and temperature were collected with the Kister9257B dynamometer and the FOTRIC infrared thermal imager (Fortic 220 series), respectively. To avoid the workpiece from surface oxidation and the consequent disturbance to the outputs of the experiments, the surface layer of the workpiece was peeled at a depth of 1 mm prior to the cutting tests.

Table 1. Relative properties of Ti-6Al-4V alloy.

Modulus of Elasticity (GPa)	Density (kg/m^3)	Yield Strength (MPa)	Poisson Ratio
114	4430	738.9	0.31

To ensure a stable cutting stage for each cutting experiment and the credibility of the experimental data, each cutting test was conducted for no less than 8 s. According to the recommended range of cutting parameters from the tool manufacturer and considering the difficult machinability of titanium alloy, medium-sized cutting parameters (a feed rate of 0.15 mm/r, cutting speed of 60 mm/min, and cutting depth of 1.0 mm) were chosen. To further improve the reliability of the experimental results, the cutting experiment in each environment was repeated three times to minimize the influences of accidental

conditions, and the total number of cutting experiments was 24. A replacement of the tool after each cutting experiment was conducted to reduce the impact of tool wear on the relevant experimental observations. After the cutting experiments, samples of the machined workpiece surface were obtained by a wire cutting machine, and the sampling method is shown in Figure 1. The surface samples were first cleaned with petroleum ether in ultrasonic cleaner and subsequently characterized after drying with respect to the 3D topography by a CTK-19-1030 white light interferometer. To investigate the wear status of the tools in different lubrication conditions, the cutting interval time was determined to be 1.25 min after multiple trials. The rake and flank wear of the tools were analyzed with an optical microscope until the flank wear in the dry cutting environment reached the wear criterion of 200 μm. Finally, the wear mechanisms of the cutting tools were investigated based on the measurement results from SEM and EDS.

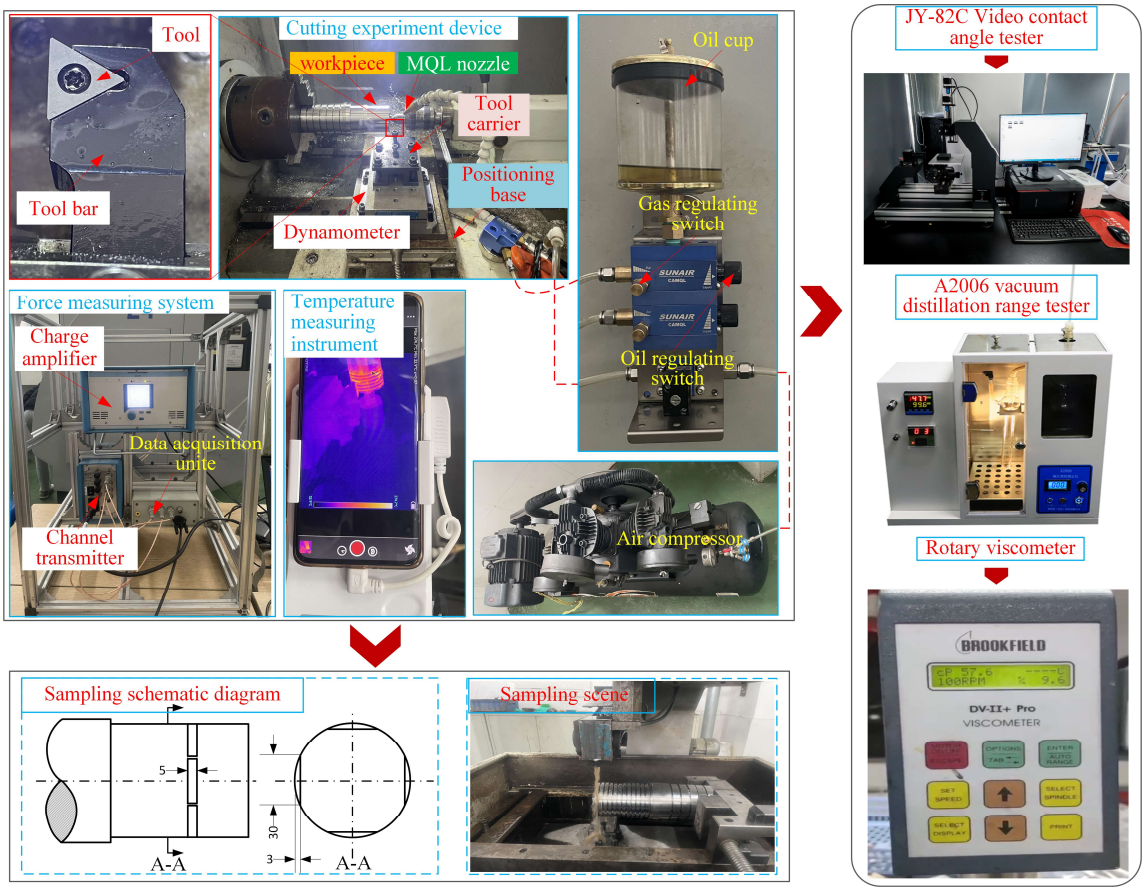


Figure 1. Platform of MQL turning experiments, detections, and analysis processes.

2.2. Testing of Thermophysical Characteristics of Cutting Fluid

Wettability is an essential factor affecting the performances of the cutting tools [25,26]. To evaluate the wettability of the tool surface with different kinds of cutting fluids, the contact angles of four cutting fluids on the rake face of the cemented carbide tool were measured by the JY-82C video contact angle tester (Figure 1). To improve the accuracy of the data, each cutting fluid was tested three times repeatedly, and the obtained average value was applied for the final analyses. In addition, the cutting tool was replaced when testing different types of cutting fluids to avoid the results of following tests being disturbed by the residual liquid on the tool rake face.

As an important characteristic of the liquids, surface tension directly affects the dynamic spreading behavior of droplets. Therefore, the surface tensions of the three vegetable

oils were measured by the drop weight method. During the measurements, the syringe containing the test liquid was placed vertically, dropping 0.8 μL of liquid each time. The dropping state of the droplet was recorded in real time, and the droplet surface tension in the stable state was measured.

In addition to wettability and surface tension, the Leidenfrost effect [27] has a serious impact on cutting fluids with respect to their cooling and lubrication properties. Cutting fluids with a low volatility can effectively reduce the Leidenfrost effect in the cutting process. In this work, the initial boiling temperatures of three kinds of cutting fluids were measured by an A2006 vacuum distillation range tester (Figure 1). The initial boiling temperature of the cutting fluid under normal pressure was obtained by converting the corresponding temperatures at low pressure.

It is known that viscosity greatly influences the flow ability of a liquid. It is difficult for liquid with high viscosity to flow at low temperatures because of the strong adhesion force. However, in the high-temperature cutting environment, viscosity decreases as temperature increases [28,29]. The forming ability of liquid film is the factor determining the lubrication and cooling performance of the liquid [30]. High-viscosity liquid can generate a thicker lubricating film [22], which is more conducive to reducing the friction coefficient of the tool–chip contact interface, thereby affecting the cutting process. To investigate the difference in the viscosity characteristics of the three cutting fluids, dynamic viscosity tests were conducted in this work at ambient temperature using a Brookfield DV-II + Pro rotary viscometer (Figure 1) with a test range of 1 cP to 6 McP and test speed of 100 r/min.

3. Results and Discussion

3.1. Comparative Analyses of Thermophysical Characteristics of Cutting Fluids

The contact angles of three cutting fluids on the tool rake face are illustrated in Figure 2, where L1 is semi-synthetic fluid and L2 and L3 are rapeseed oil and canola oil, respectively. Figure 2a–c exhibit the contact angles of L1 from the three repeated measurements, which have an average value of 41.99°. Similarly, the average contact angles of L2 and L3 were determined to be 36.69° and 39.24°, respectively. Obviously, the three cutting fluids demonstrated different wettability on the tool surface. The results reveal the best wettability of L2 on the tool rake face, followed by L3, and the relatively poor wettability of L1. However, the tool surface was hydrophilic to the three green cutting fluids, indicating that the three cutting fluids are capable for generating a lubricating film on the tool surface.

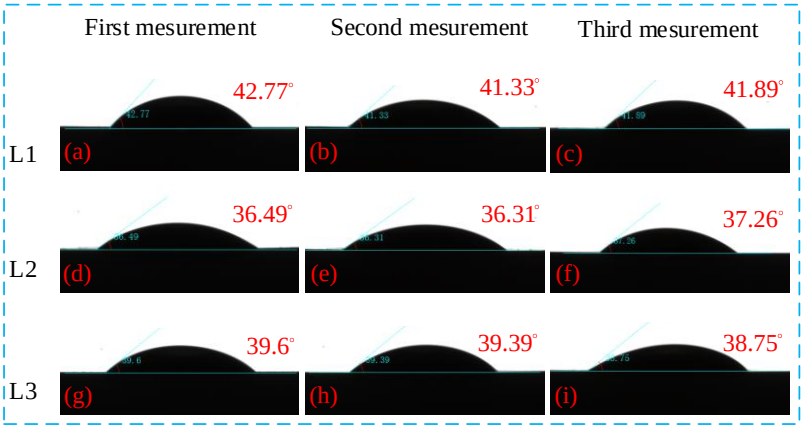


Figure 2. Contact angles of different cutting fluids on the tool rake face obtained by the first (**a**,**d**,**g**), second (**b**,**e**,**h**) and third (**c**,**f**,**i**) measurements: L1 (**a**–**c**); L2 (**d**–**f**), and L3 (**g**–**i**).

As discussed above, the contact angle can be used as a common index to evaluate the wetting and penetration abilities of cutting fluids on tool surfaces. A smaller contact angle indicates a stronger wetting effect of the fluid on the solid surface [31,32]. The spreading behavior of the cutting fluid depends largely on its surface tension, and liquids with low surface tension have a higher spreading ability [33]. The surface tensions of the three cutting fluids are presented in Figure 3. As depicted by the figures, L1 exhibited the largest surface tension, followed by L3, and the lowest surface tension was presented in the case of L2. Therefore, it could be presumed that L2 has a stronger spreading ability during the cutting process of the Ti-6Al-4V workpiece under the MQL environment, and L1 has the lowest spreading ability.

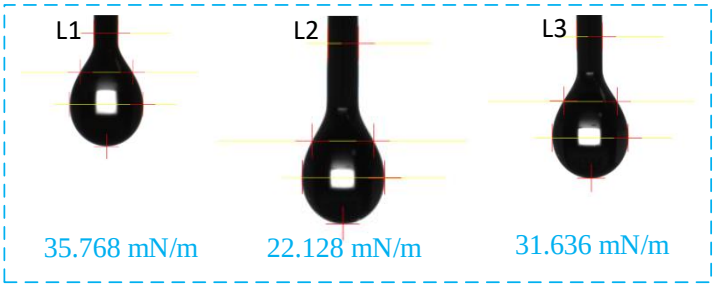


Figure 3. Surface tensions of different cutting fluids.

The lubrication and cooling effects of the cutting fluids in the cutting process depend not only closely on the surface tension and wettability of the fluids but also largely on the volatility of the fluids. The initial boiling temperatures of the fluids can be used to evaluate the volatility. A higher initial boiling temperature suggests a lower volatility of the liquid and a lower possibility of forming a gas barrier, and the liquid is more suitable for working in high-temperature environments. The initial boiling temperatures of the three cutting fluids are presented in Figure 4a. In comparison with the initial boiling temperatures of L1 (235 °C) and L3 (276 °C), L2 showed a larger value of 281 °C, indicating its higher suitability for the high-temperature cutting process from the perspective of cutting fluid volatility.

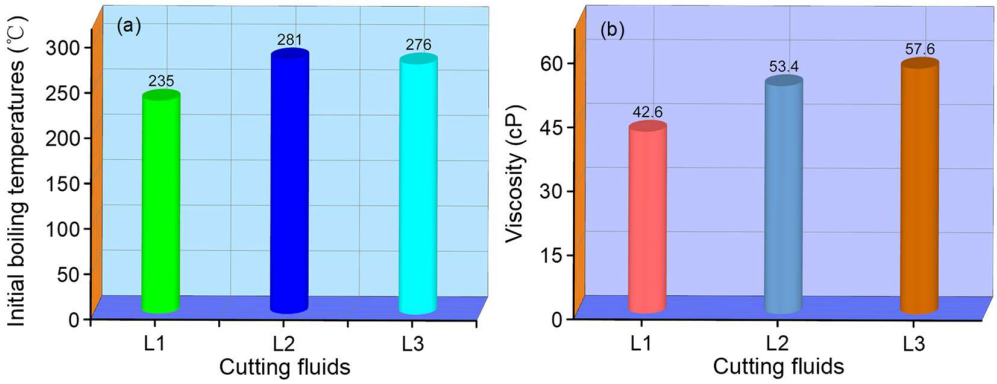


Figure 4. Comparison of initial boiling temperatures (**a**) and viscosities (**b**) of different cutting fluids.

The lubrication capability of the cutting fluid is closely correlated with the stability of the lubricating film, and viscosity can be used as an important evaluation index for the stability of the lubricating film. Figure 4b shows that L3 exhibited the highest viscosity of 57.6 cP, followed by L2 with a value of 53.4 cP, whereas L1 showed the lowest viscosity level of 42.6 cP. It is known that when increasing temperature, the viscosity of the fluid decreases. Consequently, the lubricating film formed with the low-viscosity cutting fluid would be too thin, and thus too weak in wear reduction. Meanwhile, the high-viscosity cutting fluid could form a thicker lubricating film, which can effectively enhance the lubricating

effect of the cutting fluid at the interface of the tool and the workpiece due to the higher stability of the thick lubricating film [34,35]. These analysis results demonstrate that from the aspect of fluid viscosity, L3 and L2 can offer a more effective lubrication effect than L1 in high-temperature conditions.

Comprehensive analysis showed that obvious differences in thermophysical characteristics were exhibited by the three cutting fluids, leading to differences in the cooling and lubrication effects of cutting fluids. This resulted in different cutting performances. Therefore, the cutting performances in varied cutting environments are compared and analyzed comprehensively in the next sections.

3.2. Effect of Cutting Fluid on Cutting Force

Cutting force is a typical characteristic of cutting performance, and it is also an indirect reflection of the lubrication capability of the cutting fluids. To comprehensively investigate the influences of the cutting fluids, the cutting forces at three directions were recorded during the cutting process under different lubrication environments. The resultant force is calculated as follows:

$$F = \sqrt{F_x^2 + F_y^2 + F_z^2} \tag{1}$$

where F_x, F_y, and F_z represent the cutting forces at x, y, and z directions, respectively. They could be further expressed as below:

$$F_x = \frac{1}{n}\sum_{i=1}^{n} F_{xi},\ F_y = \frac{1}{n}\sum_{i=1}^{n} F_{yi},\ F_z = \frac{1}{n}\sum_{i=1}^{n} F_{zi} \tag{2}$$

where n indicates the overall number of sampling points. The resultant forces are shown in Figure 5, in which Figure 5a exhibits that the resultant forces generated during the cutting process under the three MQL environments were reduced compared to those in the dry cutting condition, revealing the cooling and lubrication effects of the three cutting fluids. Particularly, L2 showed the largest cutting force reduction of 30.24%, followed by L3 with a decrease of 25.02%, and L1 exhibited the lowest reduction of 19.30% in cutting force. The different characteristics of the cutting fluids led to the observed variation in cutting force. The reasons for the smallest cutting force generated in the case of L2 may be caused by the following aspects: ① The initial boiling temperature of L2 is relatively high, which can effectively inhibit the Leidenfrost effect, so that the gas barrier of L2 in the cutting process is lower, thus promoting the penetration of L2. ② L2 has the lowest surface tension, which improves the spreading of L2 at the tool–chip interface. ③ High-viscosity L2 can generate a thicker lubricating film, which offers a stronger anti-friction effect. ④ In comparison with L1 and L3, L2 exhibits a smaller contact angle on the tool surface; therefore, the wettability and penetration ability of L2 are stronger. Due to the above special thermophysical characteristics, L2 showed a more superior lubrication effect and smaller cutting force in the cutting process compared to that of the other two cutting fluids.

To further verify the influences of the lubrication condition on cutting force, the correlation between cutting force and time was investigated. Figure 5b shows 12 sets of cutting force data collected with a cutting interval of 1.25 min. A basic trend of a gradual increase in the resultant force value was observed with the cutting time under all lubrication environments, which could be explained by the tool wear [36]. In the case of L2 as the cutting fluid, the average resultant force was smaller than that of the other cases, and the change in the resultant force with the cutting time was also the smallest. In contrast, the fluctuation of the resultant force in the case of L1 was relatively large. These results are highly consistent with the conclusion drawn from Figure 5a. On the other hand, the average resultant force values under the three MQL environments were always obviously

lower than that in the dry cutting process, further proving the effects of the lubrication environment on the cutting force.

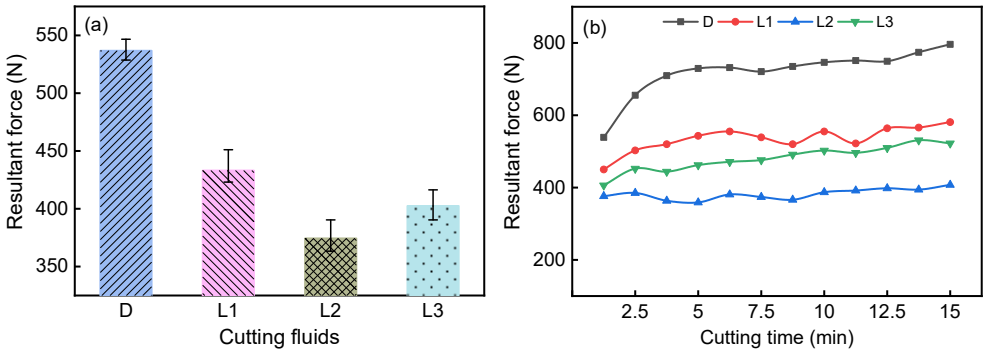


Figure 5. Effects of lubrication environment (**a**) and cutting time (**b**) on cutting force.

3.3. Effect of Cutting Fluid on Cutting Temperature

Figure 6 presents the cutting temperatures generated under varied cutting environments. The average value of the temperatures from three repeated experiments under each cutting environment was used as the final result for the analysis. As demonstrated in Figure 6a–c, the temperature reached 772.3 °C during dry cutting the Ti-6Al-4V workpiece with the given parameters. After introducing the cutting fluids into the system, the cutting temperature was reduced to some extent in all cases. The lowest cutting temperature of 666.2 °C was achieved by the introduction of L2. The addition of L3 and L1 led to cutting temperatures of 683.3 and 707.6 °C, respectively. The corresponding temperature reductions caused by using L2, L3, and L1 were 13.7%, 11.5%, and 8.4%, respectively. The cutting fluid mainly plays a role in lubricating and cooling the cutting system. Cutting fluids with a certain viscosity could form a lubricating layer at the tool–chip contact interface, thereby reducing the friction coefficient between the tool and the chip. On the other hand, cutting fluid can remove the heat generated in the cutting area through convective heat transfer, thus providing a cooling effect to some extent. The heat transferred by convection Q_c can be calculated according to Newton's law of cooling [32]:

$$Q_c = hS(T_w - T_l) \tag{3}$$

where h denotes the coefficient of convective heat transfer, T_w represents the solid temperature, T_l represents the fluid temperature, and S represents the contact area of the fluid and solid. A smaller contact angle between the fluid and solid surface means a larger contact area between the two phases and thus a greater convective heat transfer [32]. Among the three cutting fluids, L2 showed the smallest contact angle on the tool surface and lowest surface tension. This indicated a larger contact area of the fluid and solid due to the stronger wetting effect and higher spreading ability of L2, resulting in increased heat dissipation; thus, the lowest cutting temperature was achieved with L2.

In the process of cutting, the lubricating film at the tool–chip interface formed by low-viscosity cutting fluid is easy to be destroyed under the tool–chip interaction due to its insufficient thickness, which restricts the lubricating effect of the cutting fluids. Therefore, higher-viscosity cutting fluids are more suitable for high-temperature working environments compared to low-viscosity ones. In addition, the spreading characteristics and volatility of cutting fluids also have an obvious effect on the penetration of the droplets into the interface between the tool and the chip. A lower surface tension is conducive to the spreading of the cutting fluids. The higher the initial boiling temperature of the cutting fluid, the lower the possibility of forming a gas barrier, which is beneficial for the

fluid penetration at high temperatures. Under the combined effect of the above factors, L2 showed the best performance for reducing the cutting temperature, followed by L3 and L1 with a decreasing trend.

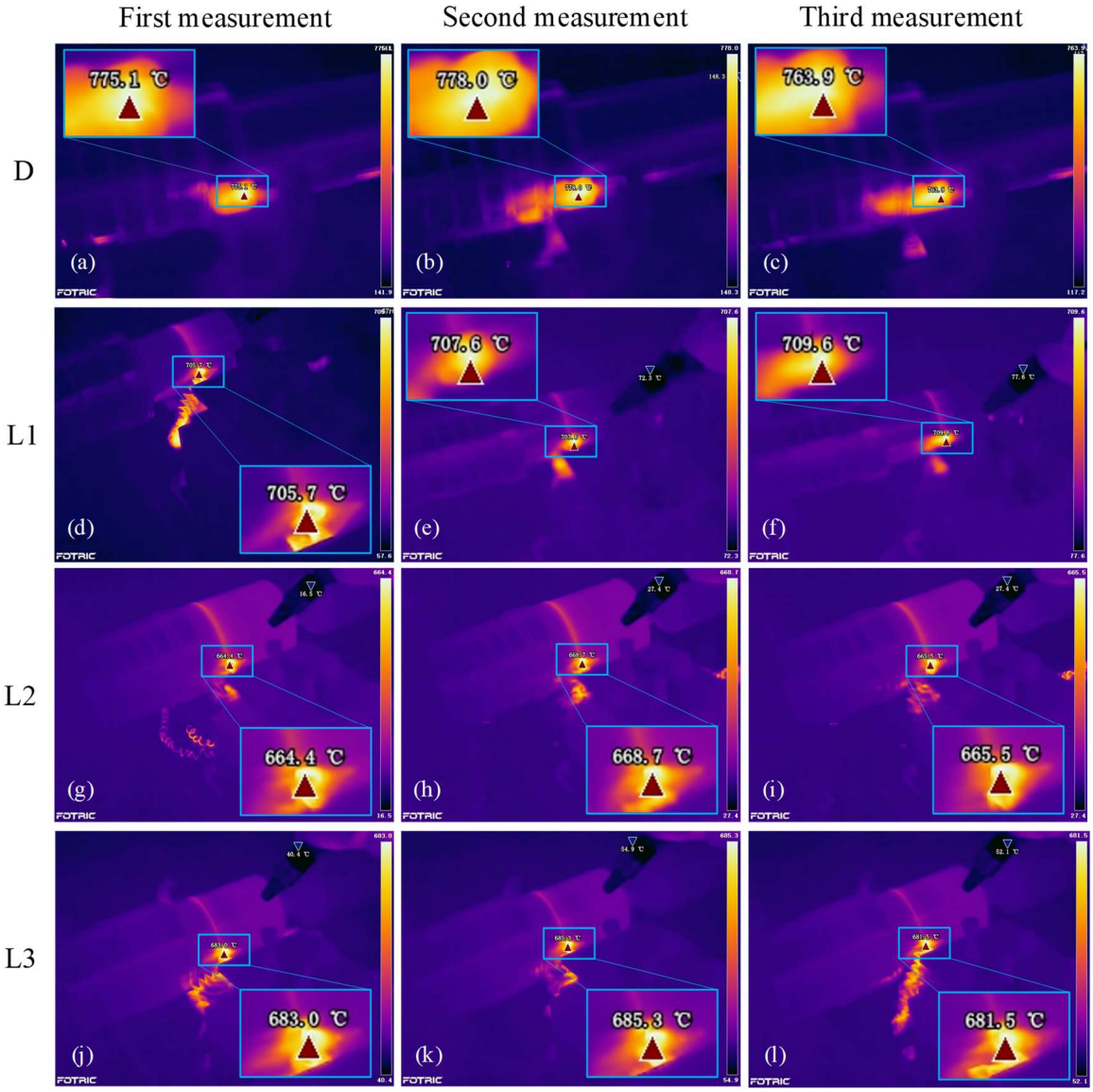


Figure 6. Cutting temperature obtained by the first (**a**,**d**,**g**,**j**), second (**b**,**e**,**h**,**k**) and third (**c**,**f**,**i**,**l**) measurements under different lubrication environments: D (**a**–**c**); L1 (**d**–**f**); L2 (**g**–**i**); L3 (**j**–**l**).

The correlation between cutting temperature and cutting time in different lubrication conditions is demonstrated in Figure 7. An upward trend in cutting temperature with cutting time was observed under all lubrication environments, and the change in the cutting temperature in the dry cutting process was most pronounced. By separately introducing the three cutting fluids into the cutting system, the cutting temperature in the MQL environment was reduced to different extents. At the same cutting time, the MQL environment with L2 performed best in the reduction in the cutting temperature, followed by the case of L3, and L1 exhibited a lower capability for a reduction in cutting temperature compared to L2 and L3. This trend is highly in line with the results from Figure 6, further confirming that the MQL environment with L2 could effectively reduce cutting temperature.

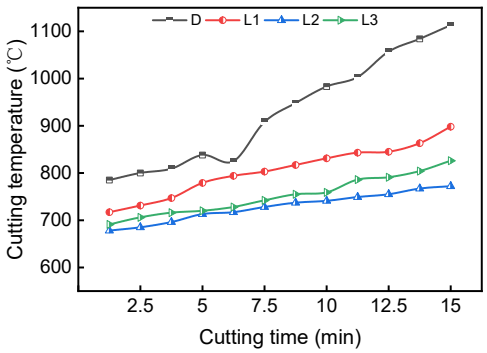


Figure 7. Effects of cutting fluid and time on cutting temperature.

3.4. Tool Wear Evolution Under Different Lubrication Environments

Tool wear is an important factor influencing the performance of the cutting tool. When tool wear exceeds a critical value, the tool will be incapable of undertaking further cutting tasks. The flank wear of cutting tools directly affects the quality of workpiece surfaces, while tool rake wear has an influence on the tool–chip interaction, thus indirectly affecting the workpiece's surface quality. With the advancement of cutting tasks, the influences of tool wear on the cutting performance are becoming more pronounced. Therefore, tool wear should be paid adequate attention during the process of cutting.

Figure 8 presents the evolution process of the tool rake wear under dry and MQL environments. The rake faces of tools in all cutting conditions exhibited obvious crater wear morphology, which could mainly be attributed to the gradient thermal load at the interface of the tool and the chip. In addition, with the extension of cutting time, the exposed worn area of the tool rake face showed a phenomenon of an alternative increase and decrease rather than a constant trend of increase or decrease. This might be correlated with chip adhesion on the tool rake face. When the chip adhesion is serious, the chip covers a larger area of the tool rake face, resulting in a decrease in the exposed worn area of the tool rake face. In contrast, when the adhered chip falls off from the tool rake face under tool–chip interaction, the exposed wear area increases. Although the rake faces of the cutting tools under the four environments all showed typical crater wear, different degrees of wear were observed. The tool rake in the dry cutting environment exhibited the most serious wear. This could be attributed to the stronger softening function of the tool material caused by the higher cutting temperatures generated during cutting in the absence of cutting fluids, which aggravated the wear close to the cutting tool edge [37]. The tool rake wear under the MQL environments with L1, L2, and L3 as the lubricants was alleviated to some extent compared to that of the dry cutting process. The degree of rake wear in the presence of L1 was higher than that in the L2 and L3 environments, and the best mitigation effect on tool rake wear was achieved with L2 as the cutting fluid.

Compared to the rake wear of cutting tools, the wear behavior of tool flank exhibited a certain degree of difference. Figure 9 presents the wear of tool flank in different cutting conditions. After the same cutting time, the largest width of the flank wear was observed in the dry cutting process, where the flank wear width reached 209 μm after 15 min, which exceeded the wear criterion of 200 μm. In comparison with the dry cutting process, the wear of the tool flank was alleviated in the three MQL environments. L2 performed the best in terms of the reduction in the flank wear, and L1 showed a lower ability of flank wear reduction than L3. Moreover, the wear widths of the tool flanks in the three MQL environments were still below the wear criterion after 15 min of cutting, indicating that the tool lifetime could be extended by using MQL technology.

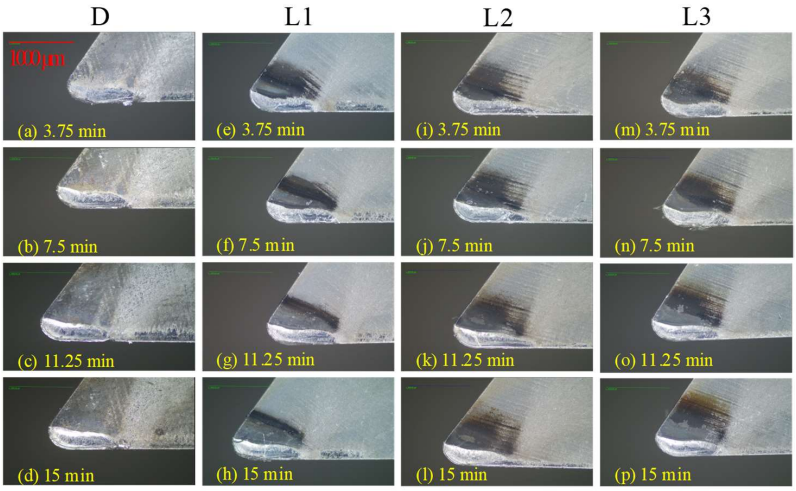


Figure 8. Evolution of tool rake wear under different lubrication environments.

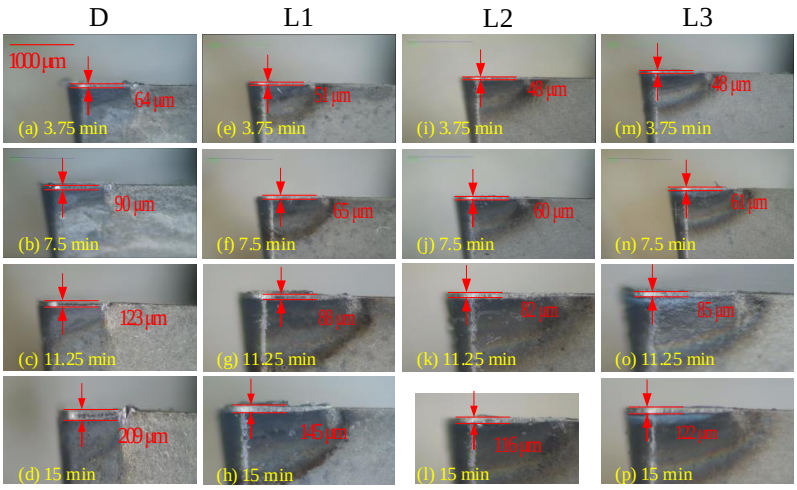


Figure 9. Evolution of flank wear under different lubrication environments.

3.5. Wear Morphology and Wear Mechanism Under Different Lubrication Environments

SEM and EDS detections were further conducted to investigate the morphologies and mechanisms of tool wear under varied lubrication environments.

3.5.1. Wear Morphology

Morphological structures of tool rake faces worn under different lubrication environments are shown in Figure 10. The tool rake faces under all cutting environments exhibited a typical crater wear morphology, highly consistent with the results obtained with the optical microscope, further proving the occurrence of crater wear. In addition, significant plastic flow of material in the crater wear area was observed. In comparison with the dry cutting process, the crater wear in the MQL environment was effectively mitigated. This was mainly because of the lower cutting force and temperature in the MQL environment, leading to smaller mechanical and thermal loads at the interface of the tool and the chip, thereby efficiently suppressing the crater wear of the tool rake face [38]. In addition, the tools under different environments formed an obvious built-up edge (BUE) at the cutting edges. The main reason for the BUE formation was that the workpiece material was subjected to strong extrusion and friction during the process of cutting. The extrusion and friction were more obvious at the chip bottom than other areas of the tool rake face because the cutting edge was in an environment with high pressure and temperature, and the flow of the surface material at the chip bottom was hindered to some extent. Therefore, the

surface material at the chip bottom adhered to the cutting edge when its friction resistance exceeded the force in the lattice structure of the material, thus forming the BUE, which was essentially the result of the cold welding in the cutting process [39]. The stable BUE could partially replace the cutting edge to perform the cutting function, thus effectively protecting the cutting edge from wear and extending the tool lifetime to some extent. However, the unstable BUE was characterized by a cycle of "formation, flaking, and re-formation" during the cutting process. This was generally unfavorable to the cutting process. Although the BUE protected the cutting edge in a short period, due to its unstable characteristic, the BUE was consistently affected by the flowing chip during cutting. With the continuation of cutting, fatigue occurred at the junction of the BUE and the cutting edge, and the BUE peeled off, thus leading to the material loss of the cutting edge and eventually the chipping phenomenon of the cutting edge. In addition, another main reason for chipping was that the cutting edge directly involved in the cutting process was located at the boundary of the chip and the workpiece surface, where it exerted a strong impact, thus leading to the chipping of the cutting edge at positions with strong impacts.

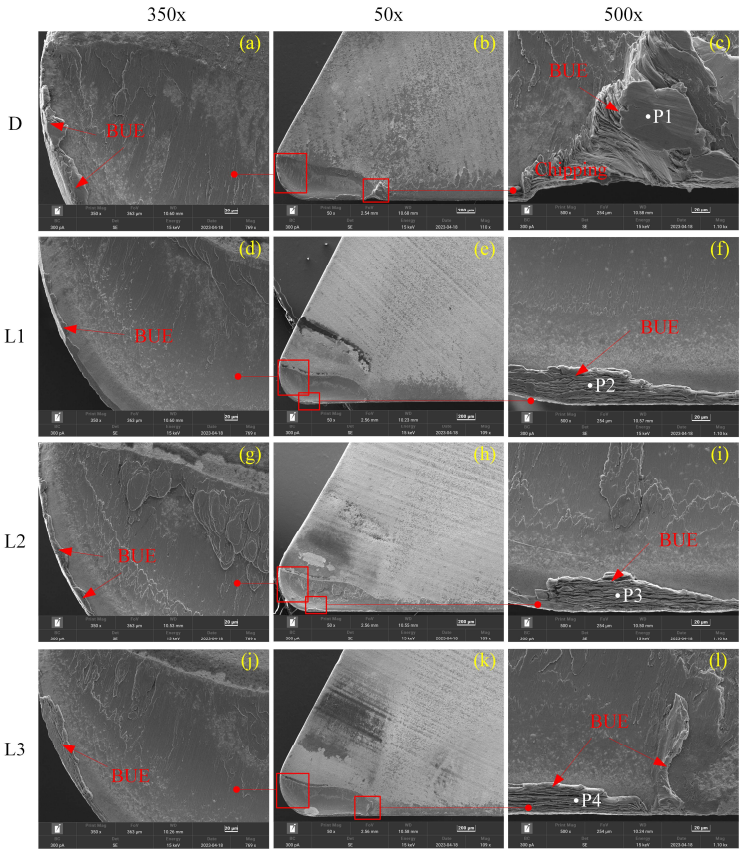


Figure 10. Morphology images of tool rake face worn in different lubrication environments: D (**a**–**c**), L1 (**d**–**f**), L2 (**g**–**i**), L3 (**j**–**l**).

As demonstrated in Figure 10c,f,i,l, the degrees of chip adhesion on the tool differed greatly under different environments. In the dry cutting environment, the adhesion volume of the chip at the tool cutting edge was significantly larger than that in the MQL lubrication environments, and the corresponding accumulation form of the chip adhesion was steep and high. In this case, the BUE was extremely unstable and easily removed by the flowing chip, which was the main reason for the obvious chipping phenomenon at the tool cutting edge during dry cutting. In the MQL environments with the three cutting fluids, the chip adhesion at the tool cutting edge was significantly weakened compared to that of the dry condition, and a more regular lamellar structure was detected. In addition, the height of

the BUE was significantly reduced in these three cases, thus improving the stability of the BUE and suppressing the BUE from peeling off. As a result, the chipping phenomenon was not observed in the three MQL environments after the tools underwent the same cutting time. Particularly, when L2 was used as the cutting fluid under the MQL environment, the chips that adhered to the cutting edge presented a lamellar feature with a lower height, higher consistency, and smaller volume than that in the L3 and L1 environments, indicating the better performance of L2 for stabilizing the BUE and protecting the cutting edge.

The morphology images of the tool flank face worn in different lubrication conditions are presented in Figure 11. Typical wear bands and distinct scratches on the flank face were observed. Their occurrences were mainly owing to the presence of some hard particles in the interaction area of the workpiece surface and tool flank face during the cutting process. The hard particles exerted a scratching effect on the tool flank face through the tool–workpiece interaction, resulting in obvious notch wear of the tool flank face. When comparing with the dry cutting process, the notch wear of the tools in the three MQL environments was effectively reduced. More specifically, the notch wear in the L1 environment was more serious than that in the L2 and L3 environments, and L2 showed the most pronounced capability for notch wear reduction. In addition, multiple micro chipping and obvious flaking of the material occurred in the tool flank face during the dry cutting process. This can be interpreted that the low thermal conductivity of the difficult-to-machine titanium alloy material caused a huge accumulation of the cutting heat generated during the cutting process, which led to a harsh mechanical impact and strong thermal stress on the cutting edge, thus resulting in voids in the tool material and the gradual formation of cracks. The gradual propagation of the crack eventually caused the lamellar detachment of the tool material.

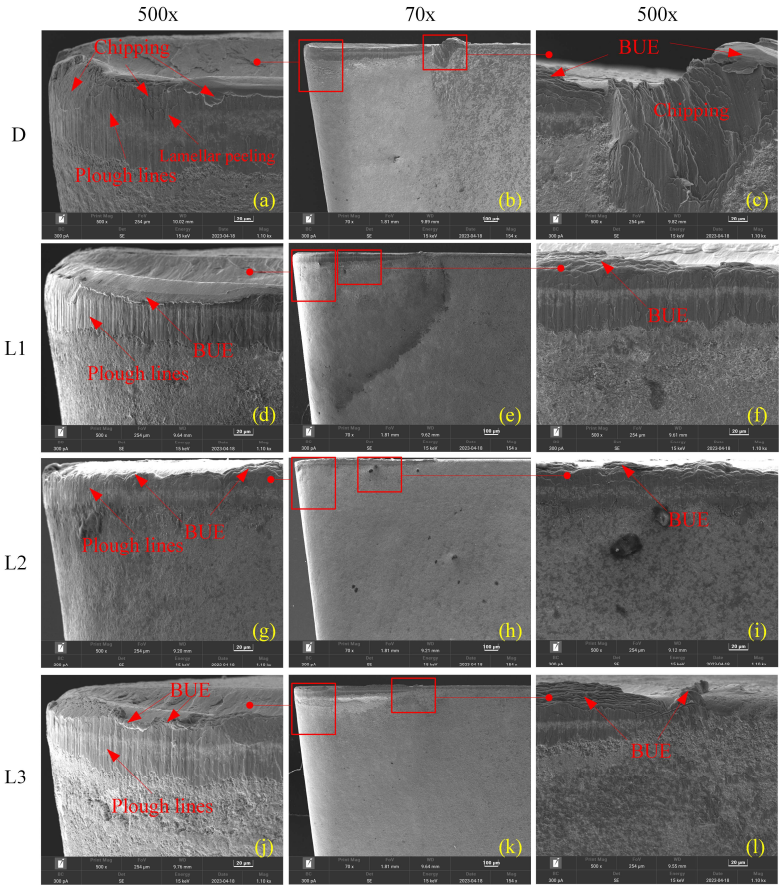


Figure 11. Morphology images of tool flank face worn in different lubrication environments: D (**a**–**c**), L1 (**d**–**f**), L2 (**g**–**i**), L3 (**j**–**l**).

3.5.2. Wear Mechanism

Wear morphology is the external manifestation of tool wear. To reveal the internal causes of tool wear, the mechanism of tool wear during the processing of titanium alloy workpieces was investigated. The energy spectra of the unprocessed tool and the workpiece in Figure 12 show that the tool comprises mainly W, Co, C, and O, with W showing the highest content in the material, while the main elements of the workpiece are Ti, Al, V, C, O, and Fe, in which Ti has the largest proportion. When tool flank wear during dry cutting reached the wear criterion, the tools after the same time of cutting under dry and MQL environments were analyzed by EDS.

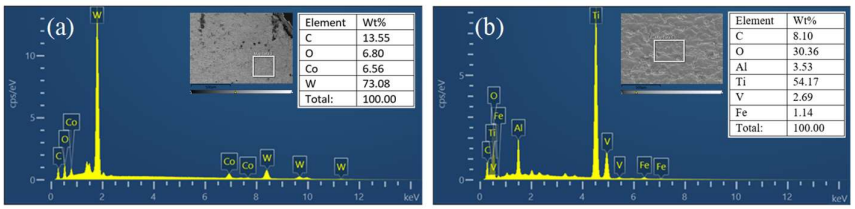


Figure 12. Main components of tool (**a**) and workpiece (**b**) before cutting.

The elemental distribution of the tool rake face after processing in dry cutting environment is presented in Figure 13. It was observed that the elements belonging to the workpiece material such as Al, Ti, and V were more densely distributed in the wear region of the rake face compared to other areas. Particularly, the density of the Ti element was significantly higher than other elements, indicating a serious adhesion of chip material on the tool rake face. In contrast, the original elements of the tool material, including W, Co, etc., appeared sparsely on the distribution map, which was mainly due to the tool surface being partially covered by the adhesive chip.

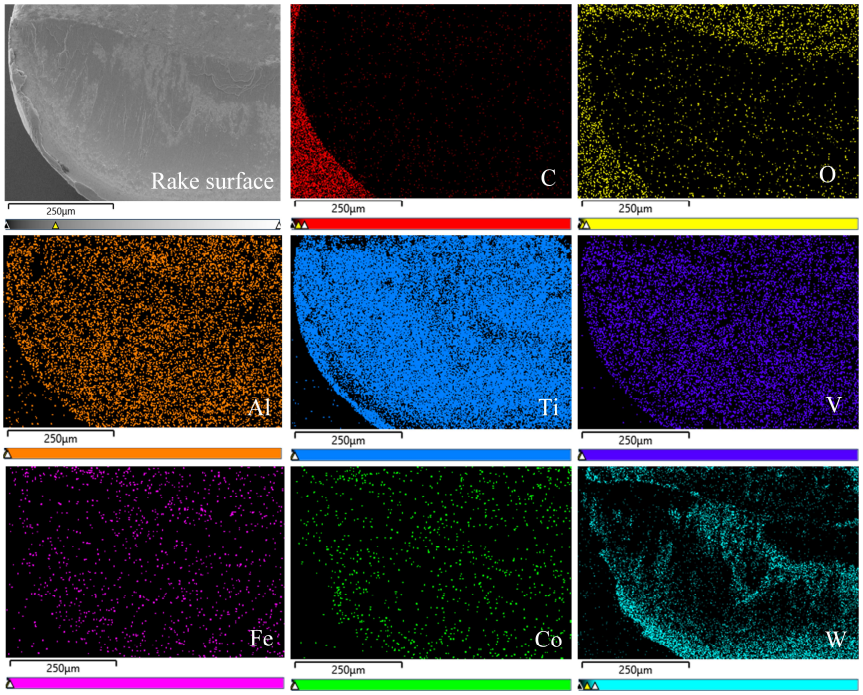


Figure 13. Element distribution of tool rake face after processing under dry cutting environment.

Since W and Ti are the main elements with the highest contents in the tool and the workpiece, respectively, the distributions of these two elements could represent the distributions of the tool and workpiece materials to the greatest extent, respectively. Therefore,

to lower the complexity of the graphics and to simplify the comparative analysis, only distributions of W and Ti elements on the tool rake face were taken into further consideration. The element distributions of the rake faces processed under different MQL conditions are presented in Figure 14, where a dense distribution of Ti in the crater wear zone of the rake face was observed, whereas W showed a relatively loose distribution in the corresponding zone, revealing a chip adhesion on the tool rake face under the three MQL environments. It is worth nothing that a highly dense distribution of the W element in the crater wear zone was detected in the L3 environment, which could be attributed to the peeling of the adhered chips from the tool matrix material.

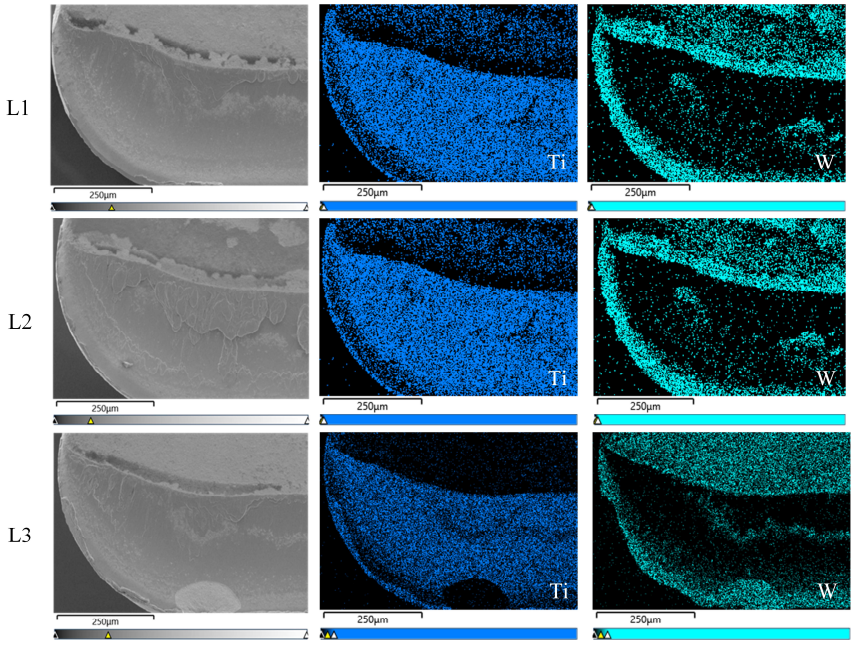


Figure 14. Element distribution of tool rake face after processing under different MQL conditions.

Figure 15 shows the element energy spectra of the tool rake faces after processing under dry cutting and different lubrication environments. The element with the highest contents in all of the four samples was determined to be Ti from the workpiece material, which is in agreement with the conclusion obtained from Figures 13 and 14, further confirming the occurrence of serious chip adhesion on the tool rake face.

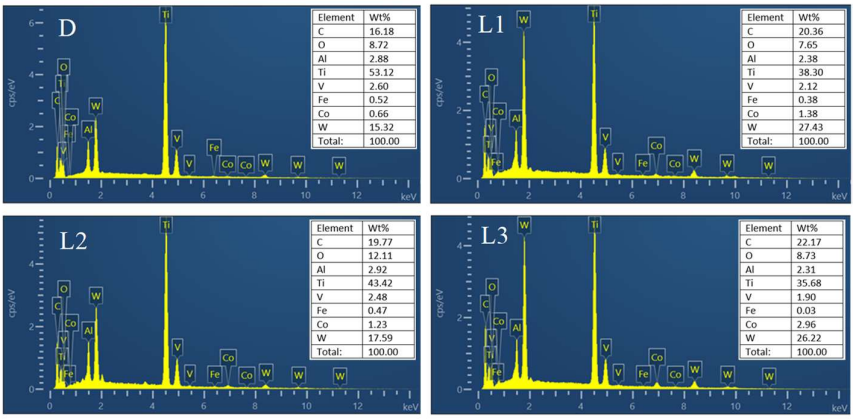


Figure 15. Elemental energy spectra of tool rake faces after processing under different lubrication environments.

EDS point scanning was performed on the adhesive material appearing on the rake face after the cutting process under different lubrication environments. The elemental energy spectra of the corresponding points marked in Figure 10 are presented in Figure 16. The main component of the adhesive material on tool rake faces after cutting in dry and the three MQL environments was Ti from the workpiece material, which showed a content around 90% in the adhesive materials, while the contents of the original tool elements such as W and Co were close to zero, indicating that the adhesive layer on the rake face was formed through the adhesion of the workpiece substance onto the cutting tool surface.

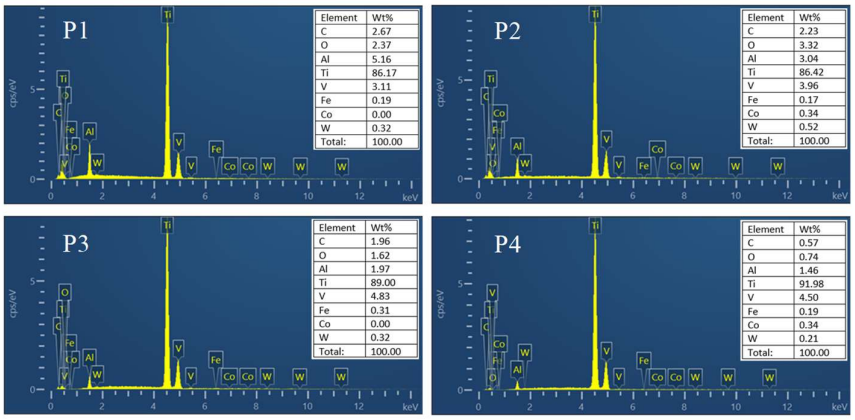


Figure 16. Elemental energy spectra corresponding to points P1, P2, P3, and P4 in Figure 10.

The element distribution and energy spectra of the tool flank faces after processing under different lubrication environments are presented in Figures 17 and 18, respectively. The main element in the selected area of the tool flank face was found to be W belonging to the tool material, which exhibited the densest distribution and the highest energy intensity in the elemental energy spectra. However, a sparse distribution of the Ti element on the tool flank face was still observed, indicating that the transfer of workpiece components also occurred on the tool flank face. In addition, the dispersion of Ti on the tool flank face was not as dense as that on the rake face under the same lubrication environment, revealing a significantly lower adhesion degree of the workpiece substance on the tool flank face compared to that on the rake face. This was mainly due to the higher mechanical and thermal loads from the first and second deformation zones on the tool rake face than the ones from the third deformation zone on the tool flank face.

In summary, different degrees of chip adhesion onto the tool flank and rake faces, as well as the cutting edge, were observed after the cutting process under different lubrication environments. When the adhesion layer reached a specific thickness value with the continuation of the cutting process, the adhered chip cracked and peeled off under the friction, extrusion generated in the second and third deformation zones, and shear forces were produced in the shear zone [40]. With the peeling of the adhesive material, the tool material was continuously removed simultaneously, leading to the adhesive wear of the cutting tools. The degree of adhesive wear on the tool rake faces was obviously larger compared to that on the flank face because of the much higher adhesion level of the workpiece substance on the tool rake face.

In addition to the adhesive wear, obvious scratches on the tool flank face were simultaneously observed by SEM detection (Figure 11). These scratches were mainly derived from some particles with much high hardness in the tool–workpiece interface. These hard particles played a role in scratching the tool surface and causing the loss of the tool flank face material, thus leading to abrasive wear. It was found that the abrasive wear of the tool flank in the dry cutting condition was more significant than that under the three MQL

environments, which followed a decreasing trend of L1 > L3 > L2. This is highly consistent with the stability of BUE formed by the chip on the cutting edge. This observation could be explained in the following way: the lower stability of BUE led to BUE being peeled off more easily during the cutting process and producing more particles, thus aggravating abrasive wear.

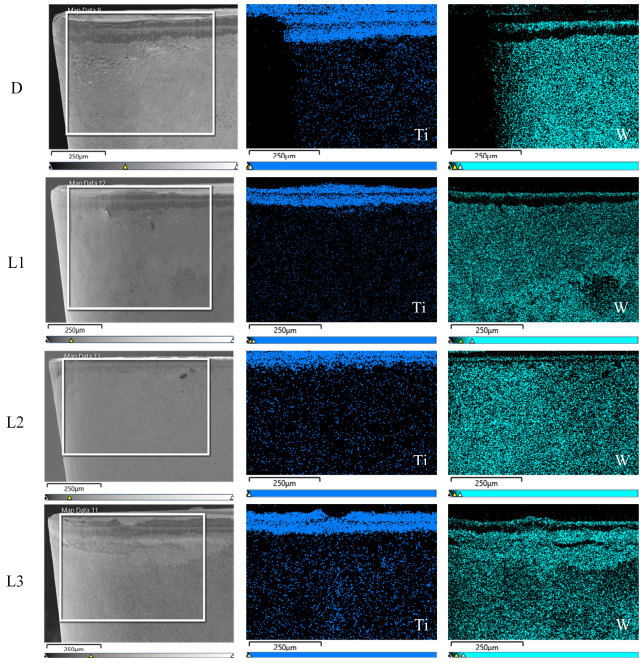


Figure 17. Element distributions of selected zone on tool flank faces in different lubrication environments.

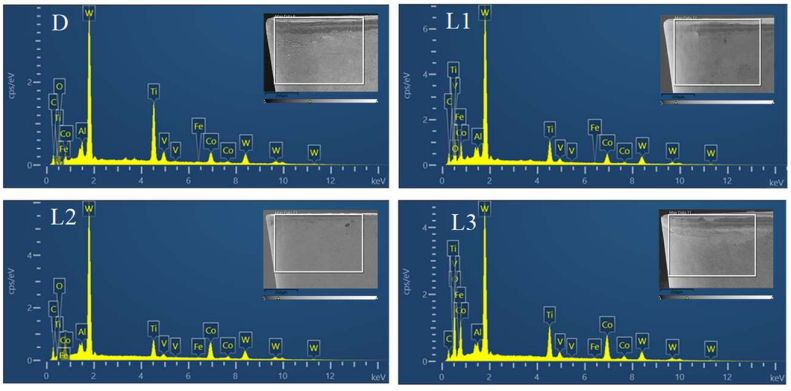


Figure 18. Elemental energy spectra of selected zone on tool flank face under different lubrication environments.

To further investigate the correlation between the tool wear degree and tool position, EDS line scanning was performed on the tool rake face and the flank face. The as-resulted distribution curves of the Ti and O elements on the tool rake face as well as the flank face in different lubrication environments are illustrated in Figures 19 and 20, respectively.

Figure 19a–d exhibit that the content of the Ti element showed a high level in the area near the main cutting edge, indicating serious adhesive wear of the tool rake face there. With the further increase in distance along the direction away from the cutting edge, the adhesive wear of the tool rake face presented a general decreasing trend, mainly due to the gradient distribution of the thermal load and mechanical load on the tool rake face. In addition, severe adhesive wear was observed in the range of 600 μm from the tool tip during dry cutting, while cutting processes under the three MQL environments effectively

reduced the adhesive wear degree and the wear range (within 250 μm from the tool tip) compared to that of the dry cutting process. Although the adhesive wear length in the case of L1 was shorter than that of the L2 and L3 environments, multiple Ti peaks at a larger distance from the tool tip were detected, indicating that the chips that adhered to the tool rake face under the L1 environment were extremely unstable and more likely to cause severe adhesive wear of the cutting tool. The ranges of severe adhesive wear in the L2 and L3 environments were almost equal, but in the range of 250 μm from the tool tip, the degree of adhesive wear in the case of L3 was greater than that in the L2 environment. These results suggest that the L2 environment could most effectively enhance the resistance of the tool rake face against adhesion wear, followed by the L3 and L1 environments, which also exhibited higher wear resistance than that of the dry cutting environment.

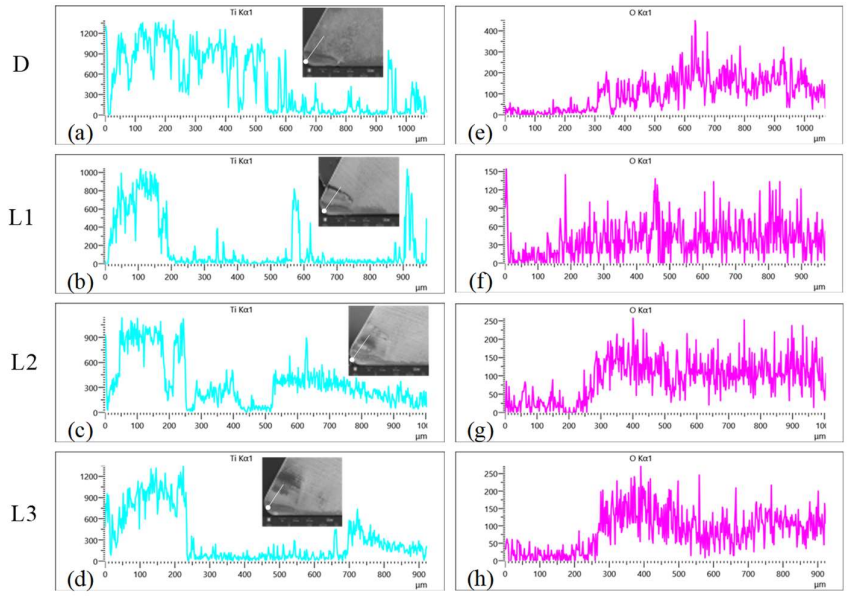


Figure 19. Distribution curves of Ti (**a**–**d**) and O (**e**–**h**) elements from line scanning on tool rake face under different lubrication environments: D (**a**,**e**); L1 (**b**,**f**); L2 (**c**,**g**); L3 (**d**,**h**).

Additionally, the correlation between the wear degree of the tool flank face and tool position was analyzed. Figure 20a–d demonstrate that there was a high level of concentration of the Ti element in the area near the main cutting edge. With the increase in the distance along the depth direction, the content of Ti was nearly reduced to zero, indicating that adhesive wear occurred only in the area near the cutting edge of the tool flank face, and there was hardly any adhesive wear at the distance far from the cutting edge. The comparison of adhesive wear degrees under different lubrication environments revealed that the tool flank face during dry cutting exhibited severe adhesive wear in the range of 90μm from the main cutting edge, whereas the introduction of the three cutting fluids effectively reduced the adhesive wear length and degree of the tool flank face. In particular, the cutting tool showed the shortest adhesive wear length of 48 μm and the lowest degree of adhesive wear on the flank face in the L2 environment. The difference in the adhesive wear length of the tool flank face in L1 and L3 environments was not significant, but the degree of adhesive wear was larger in the L1 environment. Based on the above analyses, it could be concluded that the adhesive wear on the tool rake face and the flank face was most pronounced in the dry cutting environment, followed by that of the L1 and L3 environments, and the lowest degrees of adhesive wear were achieved by using L2 as the cutting fluid under the MQL environment. This conclusion is in line with the data of cutting force and temperature under different lubrication environments.

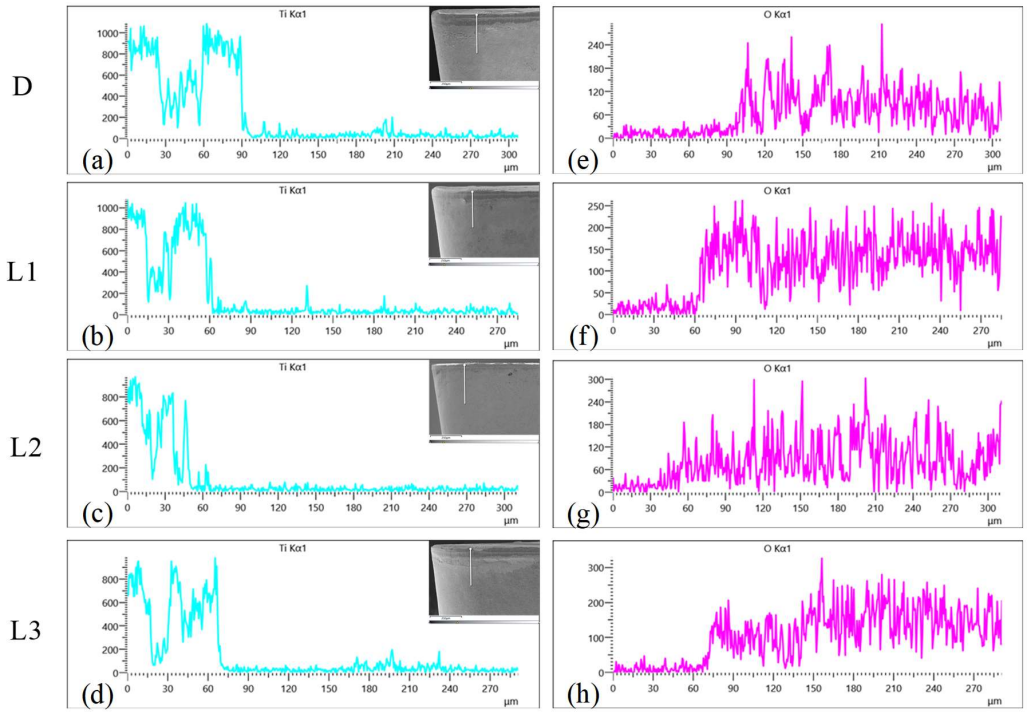


Figure 20. Distribution curves of Ti (**a**–**d**) and O (**e**–**h**) elements from line scanning on tool flank face under different lubrication environments: D (**a**,**e**); L1 (**b**,**f**); L2 (**c**,**g**); L3 (**d**,**h**).

Owing to the high system temperature derived from the cutting process of titanium alloy, the chemical activity of the tool material was enhanced. Therefore, EDS line scan analysis on the O-element content of the tool surface was performed to investigate whether the oxidative wear of cutting tools occurred. As demonstrated in Figure 19e–h, along the direction away from the tool cutting edge, the O content was nearly zero in the area near the tool cutting edge, whereas it presented a peak in the middle distance and subsequently decreased when further increasing the distance. This variation in the O element content could be explained by two aspects: ① because of the compact contact of the chip and the tool, it is difficult for air to enter the area near the cutting edge; ② owing to the gradual decrease in mechanical and thermal loads in the direction away from the cutting edge, the degree of oxidation reaction far from the tool cutting edge was also reduced, thus causing a decrease in the detected O content. In addition, the most serious oxidation wear of the tool rake face was found in the dry cutting environment, and the tool oxidation wear was reduced to some extent under the three MQL environments. The lowest wear degree was observed in the L1 environment, while the oxidative wear level in the case of L2 was larger than that in the L3 environment, which could be attributed to the different compositions and chemical stabilities of the three vegetable oils. Figure 20e–h present the distribution of the O element along the corresponding straight line on the tool flank face after processing in different lubrication conditions. Oxygen peaks were mostly observed in the middle distance region away from the cutting edge, indicating that more serious oxidative wear of the tool occurred in this zone. In contrast, the O content in the area near the main cutting edge was extremely low, which was mainly caused by the close tool–workpiece contact near the tool cutting edge, where it was difficult for air to enter, and thereby the degree of oxidative wear of the tool was low. In addition, the content of O element decreased to a certain extent at a large distance due to the lower mechanical and thermal loads at that region, which reduced the chemical activity and oxidation degree of the tool material. Therefore, oxidative wear of the tool flank face occurred mainly in the zone at medium distance away from the main cutting edge. In addition, it was also found that the oxidative

wear of the tool flank face in the L1 environment was most significant under the four lubrication environments. This may be related to its chemical composition. And the degree of oxidative wear in the dry cutting and L3 environments was similar, which was also smaller than that in the L2 environment. The different thermophysical characteristics of the three vegetable oils might be responsible for the observed phenomenon. The above experimental results reveal that the adhesive wear of cutting tools mainly occurred in the area near the tool cutting edge, whereas oxidation wear mainly took place in the middle distance area away from the tool cutting edge.

In summary, during cutting titanium alloy under both dry and MQL environments, the main wear mechanisms of tool rake faces were adhesive wear and oxidation wear, while the main wear mechanism of the tool flank face included adhesive wear, abrasive wear, and oxidation wear. Good agreement between the tool wear morphologies and the adhesive wear law was found under different lubrication environments. In terms of wear morphology, the most severe tool wear was observed during dry cutting, while the slightest tool wear was achieved in the presence of L2 under the MQL environment. With respect to the adhesive wear, it was also observed that compared to the dry cutting process, the three MQL environments remarkably improved the ability of the tool against the adhesion wear, in which L2 performed the best, followed by L3 and L1. The other observed mechanisms of wear, such as abrasive wear and oxidative wear, were relatively less significant, indicating that adhesive wear played a dominate role in the wear mechanism of cutting tools during turning titanium alloy workpieces. The multiple wear mechanisms that occurred during cutting synergistically aggravated the tool wear and caused significant changes in tool morphology, thus reducing the strength of the tool cutting edges and adversely affecting the lifetime of tools.

3.6. Quality of Machined Workpiece Surface in Different Lubrication Conditions

It is a common phenomenon that tool wear degree gradually increases with cutting time. To reduce the influence of tool wear on the surface quality of processed workpieces, the machined surface obtained after 8 s of cutting in each cutting environment was characterized. The surface roughness is a direct reflection of the surface quality of the workpieces and could be theoretically calculated as follows [41]:

$$Ra \approx 0.77R\left(1 - \frac{f_r/2R}{\arcsin(f_r/2R)}\right) \tag{4}$$

where f_r represents the feed rate and R represents the radius of the tool nose arc. It can be seen from Equation (4) that the theoretical roughness is determined by f_r and R together. However, there is usually a deviation between the theoretical surface roughness and the real roughness produced in the actual cutting process of the workpiece due to the influence of many factors such as the material characteristics of tools and workpieces, as well as the geometric angle of tools. For instance, when the composition of the tool material and the workpiece material is similar, the tool is prone to diffusion wear during the cutting process, which affects the strength of the tool and then affects the actual machined surface roughness. Figure 21 shows the surface roughness of the workpieces processed in different lubrication environments. The surface roughness values of the workpieces machined under dry cutting and the three MQL environments were larger than the theoretical roughness of 1.82 μm. The lowest actual roughness was obtained when L2 was used as the injection cutting fluid, and the value in the case of L1 was also lower than that in the dry cutting condition, while the workpiece machined under the L3 environment exhibited the largest surface roughness among the four samples.

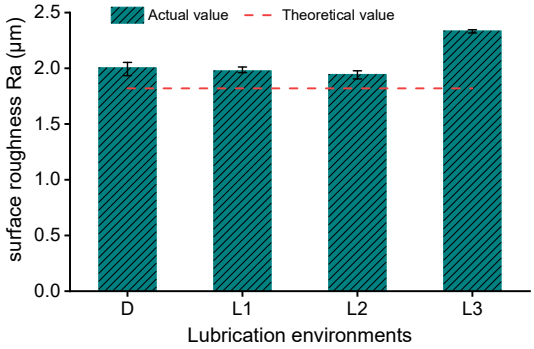


Figure 21. Surface roughness of workpieces machined under different lubrication environments.

In addition to the surface roughness that can be used as an overall evaluation index of the machined surface, 3D topography and the roughness curve in the feed direction can intuitively reflect the local details and changing trends of the machined surface. Figure 22 presents the 3D topographies and the 2D roughness profiles (in the feed direction) of the workpieces processed under different lubrication environments. Obvious peaks and valleys on the machined surface were observed in all cases, which are mainly due to the influence of tool geometry on the surface of the workpiece in the feed direction during the turning process [42]. In addition, the cycling period of peaks and valleys remains almost constant due to the fixed feed rate (0.15 mm/r) in the turning process. The largest peaks and valleys were found in the L3 lubrication environment, followed by that of the dry cutting process. The surface roughness of workpieces machined in the L1 and L2 environments showed good consistency in the feed direction, and the 3D topography obtained in the L2 environment exhibited almost no burr phenomenon in the cutting direction, maintaining a high consistency. In contrast, the 3D topography of the surface machined in other environments presented different degrees of burrs in the cutting direction, which could be the result of chip adhesion on the machined surfaces under corresponding environments.

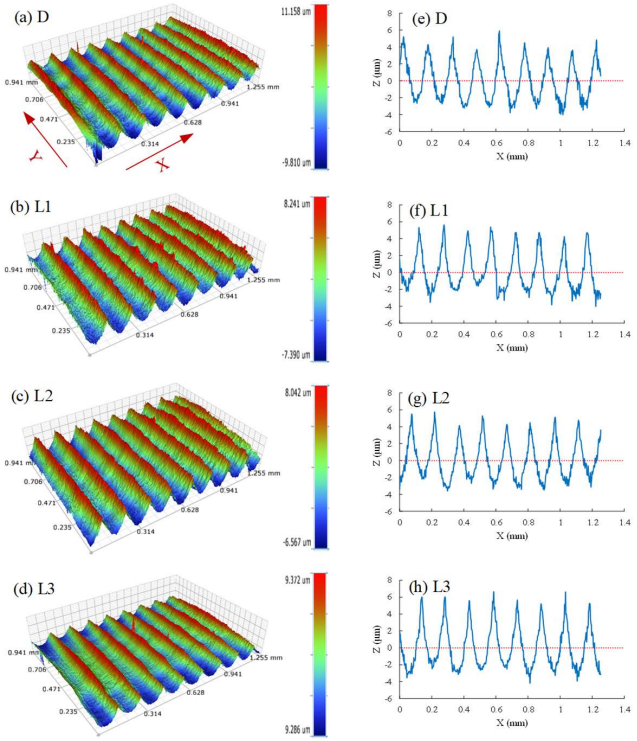


Figure 22. Three-dimensional surface topography (**a**–**d**) and two-dimensional roughness profile (**e**–**h**) of workpieces machined under different lubrication environments.

The above analyses on the average surface roughness and surface topographies of workpieces reveal that the quality of machined surfaces obtained in the dry cutting condition was higher compared to that in the L3 environment but lower compared to that under L1 and L2 environments. The reasons for this phenomenon may be related to the chemical properties of these three cutting fluids. The best machined surface quality was achieved in the case of L2, which could be related to the unique thermophysical characteristics of L2, including the relatively high initial boiling temperature and viscosity, low surface tension, as well as strong hydrophilicity on the tool surface.

4. Conclusions

To investigate the effect of the thermophysical characteristics of varied cutting fluids on the performance of cutting tools under the MQL environment, the viscosity, initial boiling temperature, surface tension, and contact angle of several green vegetable oils, including semi-synthetic fluid (L1), rapeseed oil (L2), and canola oil (L3), were first analyzed. Subsequently, the cutting performance of the tools in dry and three MQL environments was compared and evaluated from the aspects of tool wear, cutting force and temperature, and quality of machined surfaces. The conclusions of the present study are briefly summarized below:

1. Significant differences in the thermophysical properties of the three green vegetable oils were observed. L2 exhibited the lowest surface tension and smallest contact angle on the tool, revealing its best abilities in spreading on the tool surface and wetting the tool. The lubricating film formed with L3 showed a larger thickness, suggesting its higher stability. in terms of the volatility of the cutting fluid, L2 exhibited the highest initial boiling temperature and the lowest volatility; therefore, it is more suitable to be used as a cutting fluid for the high-temperature cutting process. In general, the cutting fluid with a smaller contact angle, lower surface tension, higher viscosity, and lower volatility has a stronger ability to reduce cutting force and temperature, mitigate wear, and improve surface quality.
2. The cutting forces and temperatures generated in the three MQL environments were lower than those in the dry cutting environment. The cutting forces produced in the cases of L1, L2, and L3 were reduced by 19.30%, 30.24%, and 25.02%, respectively, compared with the dry cutting environment, and the cutting temperatures generated in the cases of L1, L2, and L3 were decreased by 9.3%, 14.6%, and 12.4%, respectively, compared with the dry cutting environment. As revealed by the results, the lowest cutting force and temperature were achieved with the introduction of L2, followed by the ones in the cases of L3 and L1. The main reason for this phenomenon was the different thermophysical properties of the three green vegetable oils.
3. The dry cutting process showed the most serious tool wear and obvious micro-chipping. The three MQL environments effectively improved the wear resistance of the cutting tools. In addition, the micro-chipping phenomenon was not observed in these cases. L2 performed the best in terms of improving the wear resistance of the tools, followed by L3 which ranked second, and L1 exhibited the lowest improvement effect. In addition, the same wear mechanisms of the tools were found in both dry cutting and MQL environments. The wear mechanisms of the tool rake face were mainly adhesive wear as well as oxidation wear, and the wear mechanisms of the tool flank face mainly included adhesive wear, oxidative wear, as well as abrasive wear, among which adhesive wear played a dominant role.
4. The surface roughness of the workpieces machined in the L1 and L2 environments was smaller than that in the dry cutting environment. Particularly, the lowest surface roughness was obtained in the presence of L2, manifesting the highest surface quality

of the machined workpiece. On the other hand, although the tool wear, cutting force, and temperature in the case of L3 were lower than the corresponding values in the dry cutting process, workpieces machined in the L3 environment showed larger surface roughness and lower surface quality.

In the current study, the effects of the thermophysical characteristics of cutting fluids on the performance of cutting tools were investigated under the MQL environment. The efforts of the present study will make a contribution to the choosing of green cutting fluid in the cutting process of difficult-to-cut materials for academia and industries. In future, the effect of the chemical characteristics of cutting fluids on the machining process can be further explored.

Author Contributions: X.Z.: methodology, software, conceptualization, writing—original draft; L.H.: funding acquisition; supervision. S.Y.: data curation, investigation; J.D.: formal analysis, validation; J.Y. and Z.S.: validation; F.D.: reviewing and editing. All authors have read and agreed to the published version of the manuscript.

Funding: This work was financially supported by the National Natural Science Foundation of China (Grant No. 52265057), Higher Education Engineering Research Center of Guizhou Province (Grant No. QJJ[2023]040), and the National Natural Science Foundation of China (Grant No. 52365055).

Data Availability Statement: The data presented in this study are available on request from the corresponding author. The data are not publicly available due to restrictions of privacy.

Acknowledgments: We acknowledge the support of the National Natural Science Foundation of China (Grant No. 52265057), Higher Education Engineering Research Center of Guizhou Province (Grant No. QJJ[2023]040), and the National Natural Science Foundation of China (Grant No. 52365055). We sincerely thank the reviewers and editors for their insightful and constructive feedback, which has greatly improved the quality of this paper.

Conflicts of Interest: The authors declare that they have no known competing financial interests or personal relationships that could have appeared to influence the work reported in this paper.

References

1. Marian, M.; Almqvist, A.; Rosenkranz, A.; Fillon, M. Numerical micro-texture optimization for lubricated contacts—A critical discussion. *Friction* **2022**, *10*, 1772–1809. [CrossRef]
2. Ali, S.H.; Yao, Y.; Wu, B.; Zhao, B.; Ding, W.; Jamil, M.; Khan, A.; Baig, A.; Liu, Q.; Xu, D. Recent developments in MQL ma-chining of aeronautical materials: A comparative review. *Chin. J. Aeronaut.* **2025**, *38*, 102918. [CrossRef]
3. Xu, W.; Li, C.; Zhang, Y.; Ali, H.M.; Sharma, S.; Li, R.; Yang, M.; Gao, T.; Liu, M.; Wang, X.; et al. Electrostatic atomization minimum quantity lubrication machining: From mechanism to application. *Int. J. Extrem. Manuf.* **2022**, *4*, 042003. [CrossRef]
4. Cui, X.; Li, C.; Ding, W.; Chen, Y.; Mao, C.; Xu, X.; Liu, B.; Wang, D.; Li, H.N.; Zhang, Y.; et al. Minimum quantity lubrication machining of aeronautical materials using carbon group nanolubricant: From mechanisms to application. *Chin. J. Aeronaut.* **2022**, *35*, 85–112. [CrossRef]
5. He, T.; Liu, N.; Xia, H.; Wu, L.; Zhang, Y.; Li, D.; Chen, Y. Progress and trend of minimum quantity lubrication (MQL): A comprehensive review. *J. Clean. Prod.* **2023**, *386*, 135809. [CrossRef]
6. Tian, P.; He, L.; Zhou, T.; Du, F.; Zou, Z.; Zhou, X. Experimental characterization of the performance of MQL-assisted turning of solution heat-treated and aged Inconel 718 alloy. *Int. J. Adv. Manuf. Technol.* **2023**, *125*, 3839–3851. [CrossRef]
7. Aslan, A.; Salur, E.; Kuntoğlu, M. Evaluation of the role of dry and MQL regimes on machining and sustainability index of strenx 900 steel. *Lubricants* **2022**, *10*, 301. [CrossRef]
8. Şirin, Ş.; Sarıkaya, M.; Yıldırım, Ç.V.; Kıvak, T. Machinability performance of nickel alloy X-750 with SiAlON ceramic cutting tool under dry, MQL and hBN mixed nanofluid-MQL. *Tribol. Int.* **2021**, *153*, 106673. [CrossRef]
9. Cui, X.; Li, C.; Zhang, Y.; Ding, W.; An, Q.; Liu, B.; Li, H.N.; Said, Z.; Sharma, S.; Li, R.; et al. Comparative assessment of force, temperature, and wheel wear in sustainable grinding aerospace alloy using biolubricant. *Front. Mech. Eng.* **2023**, *18*, 3. [CrossRef]
10. Kazeem, R.A.; Fadare, D.A.; Ikumapayi, O.M.; Adediran, A.A.; Aliyu, S.J.; Akinlabi, S.A.; Jen, T.-C.; Akinlabi, E.T. Advances in the application of vegetable-oil-based cutting fluids to sustainable machining operations—A review. *Lubricants* **2022**, *10*, 69. [CrossRef]

11. Sankaranarayanan, R.; Hynes, N.R.J.; Kumar, J.S.; Krolczyk, G. A comprehensive review on research developments of vegetable-oil based cutting fluids for sustainable machining challenges. *J. Manuf. Process* **2021**, *67*, 286–313. [CrossRef]
12. Safie NS, S.; Murad, M.N.; Lih, T.C.; Azmi, A.I.; Wan Hamzah, W.A.; Danish, M. Roles of eco-friendly non-edible vegetable oils in drilling Inconel 718 through minimum quantity lubrication. *Lubricants* **2022**, *10*, 211. [CrossRef]
13. Singh, R.; Dureja, J.S.; Dogra, M.; Gupta, M.K.; Mia, M.; Song, Q. Wear behavior of textured tools under graphene-assisted minimum quantity lubrication system in machining Ti-6Al-4V alloy. *Tribol. Int.* **2020**, *145*, 106183. [CrossRef]
14. Yuan, J.; Liu, N.; Zou, X.; Wu, L.; Zhang, Y.; He, T.; Xia, H.; Wang, Y.; Chen, Y. Processing characteristics and lubrication performance of castor oil-ethanol blended coolant-based minimal quantity lubrication. *CIRP J. Manuf. Sci. Technol.* **2022**, *36*, 78–89. [CrossRef]
15. Gaurav, G.; Sharma, A.; Dangayach, G.S.; Meena, M.L. Assessment of jojoba as a pure and nano-fluid base oil in minimum quantity lubrication (MQL) hard-turning of Ti–6Al–4V: A step towards sustainable machining. *J. Clean. Prod.* **2020**, *272*, 122553. [CrossRef]
16. Du, F.; He, L.; Zhou, T.; Tian, P.; Zou, Z.; Zhou, X. Analysis of droplet characteristics and cooling lubrication effects in MQL milling of 316l stainless steel. *J. Mater. Res. Technol.* **2022**, *19*, 4832–4856. [CrossRef]
17. Subramani, S.; Muthu, S.N.; Gajbhiye, N.L. A numerical study on the influence of minimum quantity lubrication parameters on spray characteristics of rapeseed oil as cutting fluid. *Ind. Lubr. Tribol.* **2022**, *74*, 197–204. [CrossRef]
18. El-Bouri, W.; Deiab, I.; Khanafer, K.; Wahba, E. Numerical and experimental analysis of turbulent flow and heat transfer of minimum quantity lubrication in a turning process using discrete phase model. *Int. Commun. Heat. Mass.* **2019**, *104*, 23–32. [CrossRef]
19. Saleem, M.Q.; Mehmood, A. Eco-friendly precision turning of superalloy Inconel 718 using MQL based vegetable oils: Tool wear and surface integrity evaluation. *J. Manuf. Process* **2022**, *73*, 112–127. [CrossRef]
20. Guo, S.; Li, C.; Zhang, Y.; Wang, Y.; Li, B.; Yang, M.; Zhang, X.; Liu, G. Experimental evaluation of the lubrication performance of mixtures of castor oil with other vegetable oils in MQL grinding of nickel-based alloy. *J. Clean. Prod.* **2017**, *140*, 1060–1076. [CrossRef]
21. Pal, A.; Chatha, S.S.; Sidhu, H.S. Performance evaluation of various vegetable oils and distilled water as base fluids using eco-friendly MQL technique in drilling of AISI 321 stainless steel. *Int. J. Pract. Eng. Manuf. Technol.* **2022**, *9*, 745–764. [CrossRef]
22. Yin, Q.; Li, C.; Dong, L.; Bai, X.; Zhang, Y.; Yang, M.; Jia, D.; Li, R.; Liu, Z. Effects of physicochemical properties of different base oils on friction coefficient and surface roughness in MQL Milling AISI 1045. *Int. J. Precis. Eng. Manuf. Technol.* **2021**, *8*, 1629–1647. [CrossRef]
23. Jamil, M.; He, N.; Huang, X.; Zhao, W.; Khan, A.M.; Iqbal, A. Thermophysical, tribological, and machinability characteristics of newly developed sustainable hybrid lubricoolants for milling Ti-6Al-4V. *J. Manuf. Process* **2022**, *73*, 572–594. [CrossRef]
24. Nwoguh, T.O.; Okafor, A.C.; Onyishi, H.A. Enhancement of viscosity and thermal conductivity of soybean vegetable oil using nanoparticles to form nanofluids for mini-mum quantity lubrication machining of difficult-to-cut metals. *Int. J. Adv. Manuf. Technol.* **2021**, *113*, 3377–3388. [CrossRef]
25. Khanna, N.; Airao, J.; Kshitij, G.; Nirala, C.K.; Hegab, H. Sustainability analysis of new hybrid cooling/lubrication strategies during machining Ti6Al4V and Inconel 718 alloys. *Sustain. Mater. Technol.* **2023**, *36*, e00606. [CrossRef]
26. Singh, A.K.; Sharma, V. A comparative appraisal of sustainable strategy in ultrasonic assisted grinding of Nimonic 80A using novel green atomized cutting fluid. *Sustain. Mater. Technol.* **2022**, *32*, e423. [CrossRef]
27. Malinowski, R.; Parkin, I.P.; Volpe, G. Advances towards programmable droplet transport on solid surfaces and its applications. *Chem. Soc. Rev.* **2020**, *49*, 7879–7892. [CrossRef] [PubMed]
28. Dungavath, N.N.; Sharma, V. Thermophysical investigations of mango seed oil as a novel cutting fluid: A sustainable approach toward waste to value addition. *J. Manuf. Sci. Eng.* **2022**, *144*, 091004. [CrossRef]
29. Gnanadurai, R.R.; Mesfin, S. Investigations on the effect of silver nanoparticles on performance of coconut oil based cutting fluid in minimal fluid application. *Adv. Mech. Eng.* **2022**, *14*, 2072279792. [CrossRef]
30. Makhesana, M.A.; Patel, K.M.; Khanna, N. Analysis of vegetable oil-based nano-lubricant technique for improving machinability of Inconel 690. *J. Manuf. Process* **2022**, *77*, 708–721. [CrossRef]
31. Guimarães, B.; Silva, J.; Fernandes, C.; Figueiredo, D.; Carvalho, O.; Miranda, G.; Silva, F. Understanding drop spreading behaviour on Wc-10wt%Co cutting tools—An experimental and numerical study. *Colloids Surfaces A Physicochem. Eng. Asp.* **2022**, *637*, 128268. [CrossRef]
32. Lv, T.; Xu, X.; Weng, H.; Yu, A.; Niu, C.; Hu, X. A study on lubrication and cooling performance and machining characteristics of magnetic field–assisted minimum quantity lubrication using fe3o4 nanofluid as cutting fluid. *Int. J. Adv. Manuf. Technol.* **2022**, *123*, 3857–3869. [CrossRef]
33. Chetan Behera, B.C.; Ghosh, S.; Rao, P.V. Wear behavior of PVD TiN coated carbide inserts during machining of Nimonic 90 and Ti6Al4V superalloys under dry and MQL conditions. *Ceram. Int.* **2016**, *42*, 14873–14885. [CrossRef]

34. Bibin, C.; Devarajan, Y.; Bharadwaj, A.; Patil, P.Y. Detailed analysis on nonedible waste feedstock as a renewable cutting fluid for a sustainable machining process. *Biomass Convers. Bior.* **2023**, *13*, 3405–3413. [CrossRef]
35. Tuan, N.M.; Duc, T.M.; Long, T.T.; Hoang, V.L.; Ngoc, T.B. Investigation of machining performance of MQL and MQCL hard turning using nano cutting fluids. *Fluids* **2022**, *7*, 143. [CrossRef]
36. Chen, J.Y.; Liu, D.H.; Jin, T.Y.; Qi, Y. A novel bionic micro-textured tool with the function of directional cutting-fluid transport for cutting titanium alloy. *J. Mater. Process Technol.* **2023**, *311*, 117816. [CrossRef]
37. Abu Bakar, H.; Ghani, J.; Haron, C.C.; Ghazali, M.; Kasim, M.; Al-Zubaidi, S.; Jouini, N. Wear mechanisms of solid carbide cutting tools in dry and cryogenic machining of AISI H13 steel with varying cutting-edge radius. *Wear* **2023**, *523*, 204758. [CrossRef]
38. Zhao, Z.; Fu, Y.; To, S.; Zhang, G.; Lin, J. Microstructural effects on the single crystal diamond tool wear in ultraprecision turning of Ti6Al4V alloys. *Int. J. Refract. Met. Hard Mater.* **2023**, *110*, 106038. [CrossRef]
39. Sun, H.; Zou, B.; Chen, P.; Huang, C.; Guo, G.; Liu, J.; Li, L.; Shi, Z. Effect of MQL condition on cutting performance of high-speed machining of GH4099 with ceramic end mills. *Tribol. Int.* **2022**, *167*, 107401. [CrossRef]
40. Liang, J.; Gao, H.; Xiang, S.; Chen, L.; You, Z.; Lei, Y. Research on tool wear morphology and mechanism during turning nickel-based alloy GH4169 with PVD-TiAlN coated carbide tool. *Wear* **2022**, *508–509*, 204468. [CrossRef]
41. Ståhl, J.; Schultheiss, F.; Hägglund, S. Analytical and experimental determination of the Ra surface roughness during turning. *Procedia Eng.* **2011**, *19*, 349–356. [CrossRef]
42. Liang, X.; Liu, Z.; Yao, G.; Wang, B.; Ren, X. Investigation of surface topography and its deterioration resulting from tool wear evolution when dry turning of titanium alloy Ti-6Al-4V. *Tribol. Int.* **2019**, *135*, 130–142. [CrossRef]

Disclaimer/Publisher's Note: The statements, opinions and data contained in all publications are solely those of the individual author(s) and contributor(s) and not of MDPI and/or the editor(s). MDPI and/or the editor(s) disclaim responsibility for any injury to people or property resulting from any ideas, methods, instructions or products referred to in the content.